

Silicate stabilisation of colloidal UO_2 produced by uranium metal corrosion



Thomas S. Neill^a, Katherine Morris^a, Carolyn I. Pearce^{a,b}, Liam Abrahamsen-Mills^c, Libor Kovarik^b, Simon Kellet^d, Bruce Rigby^d, Tonya Vitova^e, Bianca Schacherl^e, Samuel Shaw^{a,*}

^a Research Centre for Radwaste Disposal and Williamson Research Centre, School of Earth & Environmental Sciences, The University of Manchester, Oxford Road, Manchester, M13 9PL, UK

^b Pacific Northwest National Laboratory, Richland, WA, 99354, USA

^c National Nuclear Laboratory, Chadwick House, Warrington Road, Birchwood Park, Warrington, WA3 6AE, UK

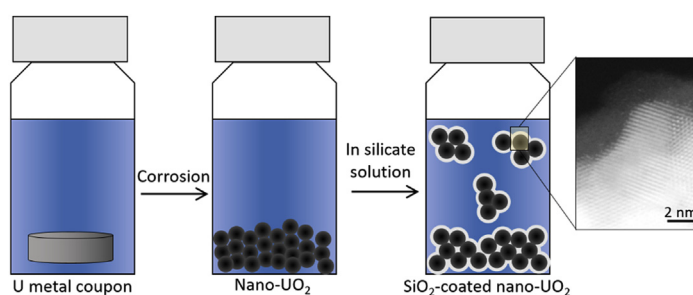
^d Sellafield Ltd., Hinton House, Birchwood Park Avenue, Risley, Warrington, Cheshire, WA3 6GR, UK

^e Institute for Nuclear Waste Disposal (INE), Karlsruhe Institute of Technology, P.O. 3640, Karlsruhe, D-76021, Germany

HIGHLIGHTS

- Product of anaerobically corroded U metal characterised as nano- UO_2 (5–10 nm).
- UO_2 forms colloids in silicate solutions, no colloids in silicate free systems.
- Particles have SiO_2 coating but maintain UO_2 core in silicate solution.
- SiO_2 coating has U atoms present suggesting UO_2 alteration at the UO_2 - SiO_2 interface.

GRAPHICAL ABSTRACT



ARTICLE INFO

Article history:

Received 24 May 2019

Received in revised form

5 August 2019

Accepted 9 August 2019

Available online 10 August 2019

Keywords:

Uranium

Silicate

Corrosion

Colloid

Coffinite

ABSTRACT

U(IV) mobility can be significantly enhanced by colloids in both engineered and natural environments. This is particularly relevant in decommissioning and clean-up of nuclear facilities, such as legacy fuel ponds and silos at the Sellafield site, UK, and in long-term radioactive waste geodisposal. In this study, the product of metallic uranium (U) corrosion under anaerobic, alkaline conditions was characterised, and the interaction of this product with silicate solutions was investigated. The U metal corrosion product consisted of crystalline UO_2 nanoparticles (5–10 nm) that aggregated to form clusters larger than 20 nm. Sequential ultrafiltration indicated that a small fraction of the U metal corrosion product was colloidal. When the uranium corrosion product was reacted with silicate solutions under anaerobic conditions, ultrafiltration indicated a stable colloidal uranium fraction was formed. Extended X-ray absorption fine structure (EXAFS) spectroscopy and high resolution TEM confirmed that the majority of U was still present as UO_2 after several months of exposure to silicate solutions, but an amorphous silica coating was present on the UO_2 surface. This silica coating is believed to be responsible for formation of the UO_2 colloid fraction. Atomic-resolution scanning TEM (STEM) indicated some migration of U into the silica-coating of the UO_2 particles as non-crystalline U(IV) -silicate, suggesting alteration of UO_2 at the

* Corresponding author.

E-mail address: sam.shaw@manchester.ac.uk (S. Shaw).

UO₂-silica interface had occurred. This alteration at the UO₂-silica interface is a potential pathway to the formation of U-silicates (e.g. coffinite, USiO₄).

© 2019 The Authors. Published by Elsevier B.V. This is an open access article under the CC BY license (<http://creativecommons.org/licenses/by/4.0/>).

1. Introduction

Uranium (U) is typically the major component by mass in spent nuclear fuels (SNF) and many radioactive wastes. U is commonly found as U(IV), either as UO₂ spent fuel [1] or from the corrosion of metallic U fuel [2–5]. U(IV) has much lower solubility than U(VI) under circumneutral and alkaline conditions [6], meaning it is often considered essentially immobile [7,8] and one of the primary barriers to prevent release of fission products and transuranics from SNF [9]. However, there is potential for U(IV) to form stable, mobile colloids which may significantly increase its mobility [10]. Colloids have been shown to mobilise radionuclides in environments such as acid mine drainage sites, where U was associated with amorphous Al-P-Fe-Si-based aggregates [11], and at nuclear weapons testing sites where Pu was likely transported via sorption to clay and zeolite colloids [12]. These studies show that colloids are important transport vectors for radionuclides in a range of scenarios. Colloids also have the potential to mobilise U(IV) and other radionuclides at legacy nuclear storage facilities such as alkaline legacy storage ponds and silos at Sellafield, UK [13]. This is particularly important during waste retrieval operations at these facilities. Here, colloidal particles may be present in effluents and their mobility within effluent processing plants is unknown. Previously, both Pu and Am were found to be associated with colloidal phases in a legacy pond effluent [14], suggesting colloidal transport is relevant to radionuclide mobility in these spent nuclear fuel storage facilities. Many of these facilities contain spent Magnox fuel, a metallic U fuel with Mg rich cladding. These facilities are maintained at an alkaline pH (e.g. pH 11–11.5 for the First Generation Magnox Storage Pond [14]), but historic issues with pond chemistry control have led to corrosion of the metallic fuel, resulting in an abundance of UO₂ [5,15]. Despite this, little is understood about the colloidal behaviour of UO₂ and other key intrinsic radionuclide containing colloids in aqueous systems of this nature.

In contact with water, metallic U corrodes to form fine UO₂ particulates [2–5]. Nanoparticulate UO₂ (<100 nm) also forms via dissolution and subsequent reprecipitation of UO₂ from thin-films under anoxic conditions [16], suggesting nanoparticulate UO₂ may be prevalent in many wasteforms including both metallic U and UO₂ based SNF. At acidic pH, UO₂ is colloidal [17,18], however at neutral and basic pH UO₂ nanoparticles aggregate and precipitate due to their reduced surface charge near the pH_{pzc} of UO₂ (5.8 [19]) which leads to a loss of colloidal stability. If aggregation is prevented then these UO₂ nanoparticles may be colloidal at high pH. Previous investigations into the anoxic corrosion of metallic U spent nuclear fuel, in silicate containing solutions, have shown that the UO_{2,08} product was nanoparticulate and, interestingly, colloidal [3]. The pH_{pzc} of these uranium corrosion product particles was reported as 2–3, which is similar to that of U(IV)-silicate colloidal particles (4–5 [20]) and much lower than that of pure UO₂ (5.8 [19]). The lower pH_{pzc} indicates that silicate may significantly affect the behaviour of UO_{2,08} colloids in this system, yet the mechanism of this corroded uranium-silicate reaction remains poorly understood. Stabilisation of colloidal nanoparticles by a surface coating of silica has previously been observed for a range of systems, including Fe(III) oxides [21], and amorphous calcium carbonate [22]. As UO₂ is also the most abundant form of U(IV) in the Earth's

crust [23], understanding these UO₂ interactions with silicate, which is ubiquitous in groundwaters [9,24], may be key to predicting U mobility in both engineered and natural environments.

Recently, U(IV)-silicate colloids have been identified as potential vectors for U(IV) transport under environmental and spent nuclear fuel storage pond relevant pH conditions (7–10.5) [13,20]. In these studies, the formation of intrinsic U(IV)-silicate colloids via reaction of dissolved U(IV) and silicate was investigated. This resulted in stable colloidal particles of approximately 5 nm, with a 1–1.5 nm UO₂ core surrounded by an amorphous U(IV)-silicate shell. These studies highlight both the strong interaction of U(IV) with silicate, and the potential for U(IV)-silicate particles to have a UO₂ component. This core-shell structure, along with the previously discussed U metal corrosion study [3] support the hypothesis of silica-coated UO₂ being a likely product of the reaction of UO₂ with silicate, and also suggests this silica coating may stabilise colloidal UO₂. However, the impact of dissolved Si on nano-UO₂ colloidal stability has not been investigated. This is relevant to U mobility in reducing environments, where U(IV) solubility is low and therefore colloidal forms of U(IV) present the greatest capacity for transport.

In addition to U mobility, U(IV)/silicate reactions are also a key factor in the long term fate of UO₂, and in the formation of secondary minerals such as coffinite (USiO₄). It has been shown previously that coffinite-like U(IV)-silicate can form on the surface of UO₂ reacted with anoxic silicate containing water, however this reaction is not fully understood [25]. Coffinite is the second most abundant U(IV) mineral yet its formation is poorly understood, with synthesis in the lab often resulting in UO₂/SiO₂/USiO₄ mixed phases [26–30]. More recently, work has shown that U(IV)-silicate particles can form from reaction of U(IV) with silicate in solution, and the resultant U(IV)-silicate species may play an important role in coffinite formation [13,29].

A comprehensive understanding of the products of U metal corrosion, and how these phases interact with silicate, is essential when considering the mobility of radionuclides in nuclear wastes. Information on the potential for colloid formation, the structure of the colloids, and on interactions between U(IV) particles and silicate are crucial for safe handling and disposal of nuclear waste that contains these species. Here, we characterise the products of metallic uranium corrosion formed under anaerobic, alkaline conditions, and investigate the reaction between the U corrosion products and silicate solutions. Particle size was analysed using ultrafiltration coupled to inductively coupled plasma mass spectrometry and atomic emission spectroscopy (ICP-MS and ICP-AES) and transmission electron microscopy (TEM), and particle structure using scanning TEM (STEM), X-ray absorption spectroscopy (XAS) and X-ray diffraction (XRD).

2. Methods

2.1. Characterising U metal corrosion product

Preweighed metallic U (10 g) was washed using deoxygenated acetone in an anaerobic cabinet. The metallic U was corroded by anaerobic reaction with 0.001 M NaOH at 50 °C for approximately 200 days to form the U corrosion product used in this study. After ~200 days when corrosion was complete, as indicated by the

cessation of H₂ formation, the samples were separated into plastic containers and stored in a hermetically sealed anaerobic atmosphere at room temperature for 3.5 years prior to analysis.

All subsequent manipulations were carried out in an anaerobic cabinet (95% N₂/5% H₂) with an O₂ content of <20 ppm to prevent oxidation of U(IV). All solutions were made from degassed, deionised water (18 MΩ).

Samples of the U corrosion product were received as a wet slurry in a pH 11 NaOH supernatant, stored in sealed containers. To separate the solid from the supernatant, the U corrosion product was centrifuged at 4000 g for 10 min and supernatant extracted. An aliquot of the separated supernatant was sequentially filtered using polyethersulfone (PES) 0.22 μm syringe filters and 300 and 3 kDa PES ultracentrifuge filters (approximately 12 and 1.5 nm pore size respectively [20,31,32]). Total Si and U concentrations in the filtrate were analysed using ICP-AES (Perkin-Elmer Optima 5300 dual view) and ICP-MS (Agilent 7500cx) respectively. TEM samples of the unfiltered supernatant were prepared by dropping 5 μL of the supernatant onto a holey carbon copper TEM grid followed by washing with degassed, deionised water. TEM analysis was performed using an FEI TF30 analytical FEG TEM running at 300 kV equipped with an Oxford Instruments Silicon Drift Detector EDS system using Oxford INCA software.

For powder XRD, a sample of U corrosion product solid was washed by resuspension in degassed, deionised water, centrifuged, the solid isolated, resuspended in isopropanol and added dropwise to an XRD slide. The sample was stored in a poly(methyl methacrylate) anaerobic sample holder (Bruker) prior to, and during analysis. The sample was scanned from 5 to 70° 2θ, with a step size of 0.02° and a count time of 0.2 s per step with Cu Kα X-rays with a wavelength of 1.5406 Å. U L₃ edge XAS samples were prepared by isolating particles from solution on 3 kDa filters and mixing with cellulose to ~1 % U concentration [13]. Samples were analysed on Diamond Light Source B18 beamline in transmission mode at liquid nitrogen temperature. Data were analysed using the Demeter software package Athena and Artemis and FEFF6 [33].

2.2. Reaction of U corrosion product with silicate solutions

Silicate solutions were prepared by dissolution of sodium metasilicate nonahydrate (Na₂SiO₃·9H₂O) in degassed, deionised water and adjusted to pH 11 using NaOH (1.5 M). Samples of the centrifuged U corrosion product slurry were added to silicate solutions across a range of U and Si concentrations. Details of the composition of these samples are shown in Table 1. Total Si and U concentrations of the unfiltered, agitated suspensions were analysed using ICP-AES and ICP-MS respectively. The pH was monitored immediately after addition of U corrosion product to verify no change in pH occurred. Experiments were sampled at select intervals for ultrafiltration, TEM and XAS analyses. Experiments were ultrafiltered immediately after shaking at 1, 6, 20 and 30 week time points, as described in section 2.1 using 0.22 μm, 300 and 3 kDa filters. The impact of particle settling was also investigated on the 30 week aged samples. Here, samples were shaken and aliquots of the

supernatant were taken 0, 1 and 48 h after shaking and ultrafiltered to monitor the effect of settling on supernatant particle size distribution. STEM analysis of 8 week aged samples (supernatant and bulk) was carried out on a probe corrected FEI Titan 80–300 operated at 300 kV. All images were digitally recorded using high-angle annular dark-field (HAADF) detector. The imaging conditions were set such that the probe convergence angle was 18 mrad, and the inner detection angle on the HAADF detector was three times higher than the probe convergence angle.

U L₃ edge XAS samples of the silicate reacted U corrosion product (at 1 week and 20 weeks) were prepared and analysed as described in section 2.1. To further probe the U oxidation state in these samples, high energy resolution fluorescence detected XANES (HERFD-XANES) analysis was carried out at the ACT station of the CAT-ACT beamline, KIT synchrotron radiation source using a Si (1 1 1) double crystal monochromator [34]. For HERFD-XANES, a sample from Experiment 1 (8.6 mM Si, 0.9 mM U, Table 1) was collected on a 3 kDa filter. The U M₄ edge was measured using the M_β fluorescence line diffracted using a Johann-type spectrometer with 4 analyser crystals (Si 2 2 0); bending radius 1 m; Bragg angle 75.2°) along a Rowland geometry with 1 m radius.

3. Results and discussion

3.1. U corrosion product characterisation

U L₃ edge XANES spectroscopy of the U corrosion product solid was consistent with U(IV) dominating (Fig. S1) and EXAFS fitting confirmed UO₂ was the only discernible phase (Fig. 1, Table 2). EXAFS fitting showed a U-U coordination number in the first U shell of 12, which is expected for fully crystalline UO₂, and the presence of clear peaks in the Fourier transformed EXAFS at R > 5 Å are consistent with multiple U-U shells and a highly crystalline particle structure. These results are in agreement with previous investigations into the corrosion of metallic uranium [3], in which TEM analysis revealed that UO₂ nanoparticles of 5–10 nm aggregated into larger structures. This was supported by XRD analysis of the corrosion product (Fig. S2), which showed a diffraction pattern consistent with UO₂, with a unit cell size of 5.470 Å suggesting

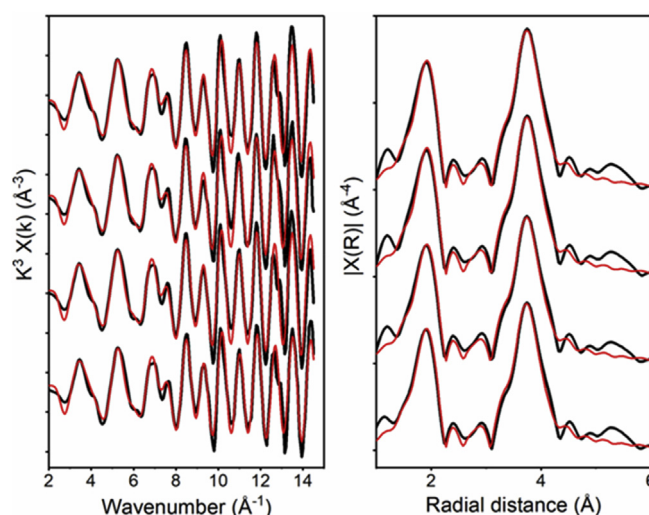


Fig. 1. EXAFS (left) and Fourier transformed EXAFS (right) of 20 week aged samples of silicate reacted U corrosion product and original U corrosion product sample. From top to bottom: silicate reacted U corrosion product Experiment 1, 2, 3 and unaltered U corrosion product. Spectra are in black with fits overlaid in red. (For interpretation of the references to colour in this figure legend, the reader is referred to the Web version of this article.)

Table 1

Composition of silicate reacted U corrosion product experiments. U and Si concentrations were taken from an aliquot of the shaken experimental mixture. All experiments were carried out at pH 11.

| Experiment | [Si]/mM | [U]/mM | Si:U molar ratio |
|------------|---------|--------|------------------|
| 1 | 8.6 | 0.9 | 9.3 |
| 2 | 3.3 | 0.4 | 8.5 |
| 3 | 1.6 | 0.5 | 3.2 |
| 4 | 0 | 1.1 | 0 |

Table 2
EXAFS fitting parameters for all samples.

| Experiment | Age / wk | R factor | S0 ² | ΔE_0 (eV) | O1 | R (\AA) | | | σ^2 (\AA^2) | | |
|---------------------|----------|----------|-----------------|-------------------|---------|--------------------|---------|----------|-------------------------------|----------|--|
| | | | | | | U | O2 | O1 | U | O2 | |
| 4 | 1 | 0.0090 | 0.83(6) | 6.0(7) | 2.36(1) | 3.88(1) | 4.46(1) | 0.007(1) | 0.004(1) | 0.010(2) | |
| 3 | 1 | 0.0098 | 0.85(7) | 6.6(7) | 2.36(1) | 3.88(1) | 4.46(2) | 0.007(1) | 0.004(1) | 0.010(3) | |
| 2 | 1 | 0.0103 | 0.92(8) | 6.6(7) | 2.36(1) | 3.88(1) | 4.46(2) | 0.007(1) | 0.004(1) | 0.010(3) | |
| 1 | 1 | 0.0095 | 0.92(7) | 6.4(7) | 2.36(1) | 3.88(1) | 4.46(1) | 0.007(1) | 0.004(1) | 0.009(2) | |
| 3 | 20 | 0.0095 | 0.92(7) | 6.2(7) | 2.36(1) | 3.88(1) | 4.46(1) | 0.007(1) | 0.004(1) | 0.010(2) | |
| 2 | 20 | 0.0126 | 0.89(7) | 6.1(7) | 2.36(1) | 3.88(1) | 4.46(2) | 0.006(1) | 0.004(1) | 0.010(2) | |
| 1 | 20 | 0.0092 | 0.92(7) | 6.2(7) | 2.36(1) | 3.88(1) | 4.46(1) | 0.007(1) | 0.004(1) | 0.009(2) | |
| U corrosion product | | 0.0099 | 0.85(7) | 6.6(7) | 2.36(1) | 3.87(1) | 4.45(2) | 0.007(1) | 0.004(1) | 0.010(3) | |

R denotes atomic distance; σ^2 denotes Debye – Waller factor; ΔE_0 denotes the shift in energy from the calculated Fermi level; S0² denotes the amplitude factor; R factor denotes “goodness of fit”. Coordination numbers were fixed to 8 (O1), 12(U) and 24(O2) for all fits. Numbers in parentheses are the standard deviation on the last decimal place.

stoichiometric UO₂ [35].

Ultrafiltration analysis of the U corrosion product supernatant after centrifugation (10 min at 4000 g) and separation indicated the vast majority of the colloidal U (11 ppm) was present in particles greater than 220 nm in size (Fig. S3). 0.6 ppm U was in the 220–1.5 nm size range and 0.5 ppm U in the <1.5 nm fraction. Solution analysis also identified 0.1 ppm Si was present in particulates (>1.5 nm) and not present in the solution (<1.5 nm) fraction. This trace level Si, likely an artefact from dissolution of the glassware at alkaline pH during the original corrosion experiment, was assumed to be associated with U particulates. TEM imaging of the U corrosion product supernatant showed a wide range of aggregate sizes between 20 and >1000 nm (Fig. 2). These aggregates were made up from 5 to 10 nm primary particles, and occasionally separate individual particles were identified. Energy dispersive X-ray (EDX) spectroscopy confirmed the imaged particles were U-rich. Fe

detected from EDX analysis was an artefact of background Fe in the TEM. Lattice fringes, indicating crystalline particles, were observed and selected area electron diffraction (SAED) patterns show UO₂ is the dominant crystalline product. After initial characterisation of the U corrosion product, samples were reacted with silicate solutions to probe the influence of silicate on U corrosion product colloid stability and particle structure.

3.2. U corrosion product-silicate characterisation

Ultrafiltration results from silicate reacted U corrosion product experiments showed clear differences between the silicate containing and silicate free experiments. Between 2.8 and 4.6% U and 3.1–3.7% Si were present in the 1.5–220 nm size fraction in all the silicate containing experiments (Experiments 1–3) at 1 week (Fig. 3). By contrast, <0.1% U was present in this fraction in the silicate free experiment (Experiment 4). In all cases, most of the Si was in the solution fraction (<1.5 nm), with more in the >220 nm size fraction, than the 1.5–220 nm size fraction, which is also true for the U size distribution. In the absence of U corrosion product, detectable Si was only present in the solution fraction (<1.5 nm). These results are consistent with silicate being present either as a dissolved species, or associated with the U particulates. The amount of dissolved U (<1.5 nm) was between 1.8 and 2.1 μM (0.2–0.5% of the total U) across the 4 experiments, which is above the predicted

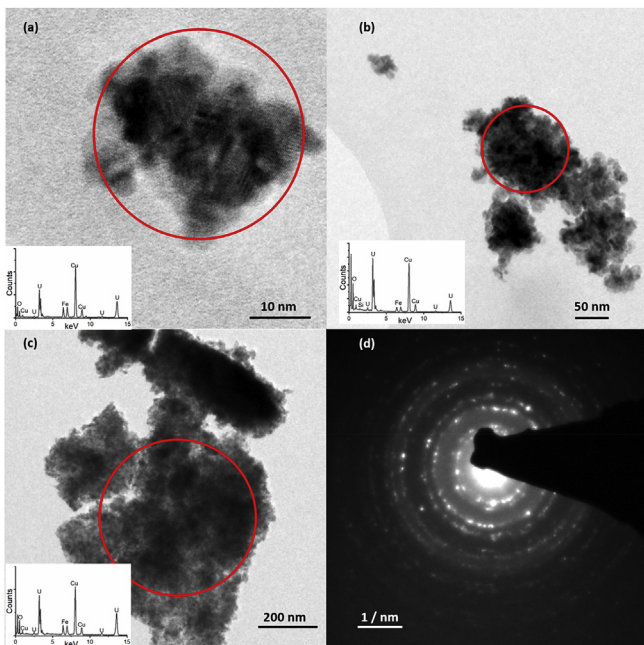


Fig. 2. TEM images of a U corrosion product supernatant particles, circles showing location of EDX spectra showing elemental composition of the particles. (a) Shows primary particles of 5–10 nm size within larger aggregates, and the presence of lattice fringes indicating a crystalline structure. (b) and (c) show the presence of larger aggregates and SAED of particle (c) is shown in (d) with a diffraction pattern indicative of nanocrystalline UO₂.

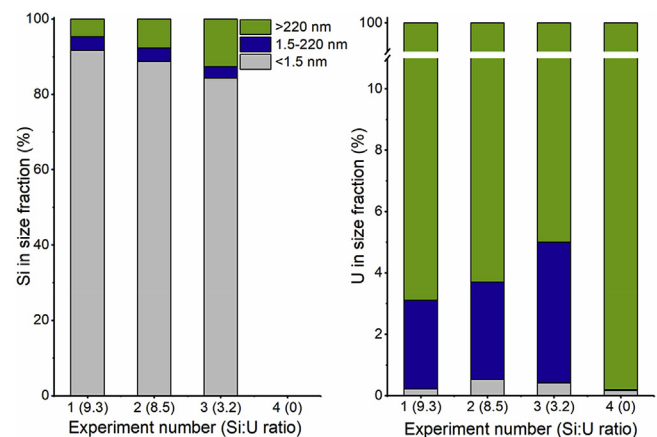


Fig. 3. Ultrafiltration results for silicate reacted U corrosion product after 1 week reaction showing Si size distribution (left) and U size distribution (right). (Experiment 1 = 8.6 mM Si, 0.9 mM U, 2 = 3.3 mM Si, 0.4 mM U, 3 = 1.6 mM Si, 0.5 mM U and 4 = 0 mM Si, 1.1 mM U).

solubility of $\text{UO}_2(\text{am})$ at pH 11 (0.003 μM) [36]. This is likely due to a small amount of oxidation of the sample (<0.5%), resulting in more soluble U(VI) species.

In the silicate containing experiments (Experiments 1–3, Table 1), U remained present in the 1.5–220 nm size fraction over 30 weeks, with <0.1 ppm U in this size fraction in the silicate free experiment (4) (Fig. 4). Generally, in silicate containing experiments, the amount of 1.5–220 nm U was stable over time at concentrations of between 2.5 and 6.5% of the total U. To identify whether the U present in this particle size fraction was colloidal, supernatant samples were ultrafiltered at set time points after shaking at 30 weeks (Fig. 5). The amount of 1.5–220 nm U particulates in the supernatant was measured at three settling times; 0, 1 and 48 h after shaking. The results shown in Fig. 5 show a stable population of 1.5–220 nm particles in Experiments 1–3 that does not decrease over time, confirming that particles of this size do not

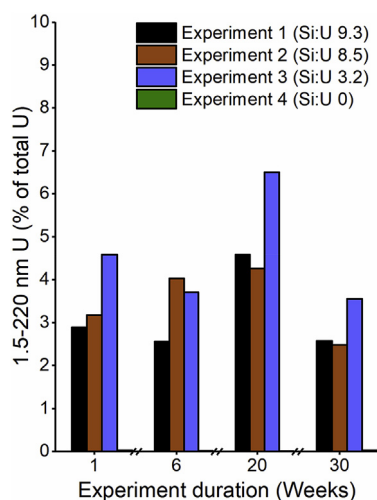


Fig. 4. Filtration results showing % of U in the 1.5–220 nm size fraction for the silicate reacted U corrosion product systems for 1, 6, 20 and 30 week time points. (Experiment 1 = 8.6 mM Si, 0.9 mM U, 2 = 3.3 mM Si, 0.4 mM U, 3 = 1.6 mM Si, 0.5 mM U and 4 = 0 mM Si, 1.1 mM U).

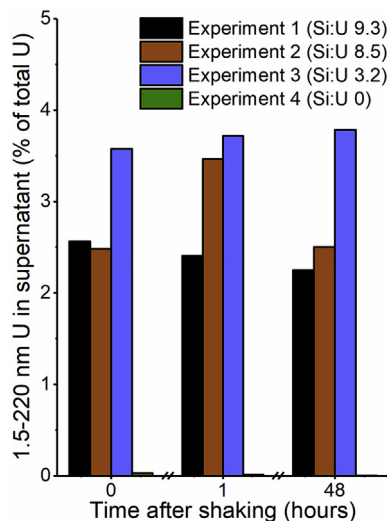


Fig. 5. Percentage of total U present as 1.5–220 nm particles in the supernatant of the silicate reacted U corrosion product experiments, 0, 1h and 48 h after shaking (30 week sample). (Experiment 1 = 8.6 mM Si, 0.9 mM U, 2 = 3.3 mM Si, 0.4 mM U, 3 = 1.6 mM Si, 0.5 mM U and 4 = 0 mM Si, 1.1 mM U).

settle out and are colloidal. TEM images show the primary particles of both the initial U corrosion product (Fig. 2) and the silicate reacted U corrosion product (Fig. 6) to be < 12 nm in size however U particles in the 1.5–12 nm size fraction were not observed in the ultrafiltration results (additional ultrafiltration results including 1.5–12 and 12–220 nm fractionation are shown in Fig. S4). The 1.5–220 nm U in these systems was almost exclusively in the 12–220 nm size fraction, indicating the aggregates observed via TEM are present in the suspensions, but the independent primary particles are not. Given the absence of U in the <220 nm particulates in the silicate free system, it is apparent that silicate is causing disaggregation of large, >220 nm U corrosion product aggregates, leading to formation of these smaller, but still aggregated, 12–220 nm particles.

High-angle annular dark-field (HAADF) STEM imaging was used alongside standard TEM imaging to identify U due to its high atomic number and the high z-contrast relative to silica (Fig. 5). After 8 weeks aging in silicate solutions, HAADF imaging and bright field TEM showed that the particles had retained their highly crystalline UO_2 structure, with visible lattice fringes. SAED patterns recorded were consistent with a UO_2 structure, and 5–10 nm primary particles, aggregated into larger structures, were once again prevalent. Importantly though, amorphous regions were observed in some areas at the edges of particles and these regions showed much lower brightness in the HAADF imaging, suggesting they were made up of lighter elements e.g. Si and O. EDX analysis confirmed the collocation of U and Si in these particles with Si apparently present as a coating (Fig. 6). While some areas of the silica coating were up to 5 nm thick, other regions showed little or no silica coverage, suggesting heterogeneous coverage (Fig. 6c).

Using HAADF imaging it was possible to observe the silica coating on the U corrosion product particles and also observe bright spots within the coating, attributed to the presence of individual U atoms present in this silica coating. This suggests that some of the U

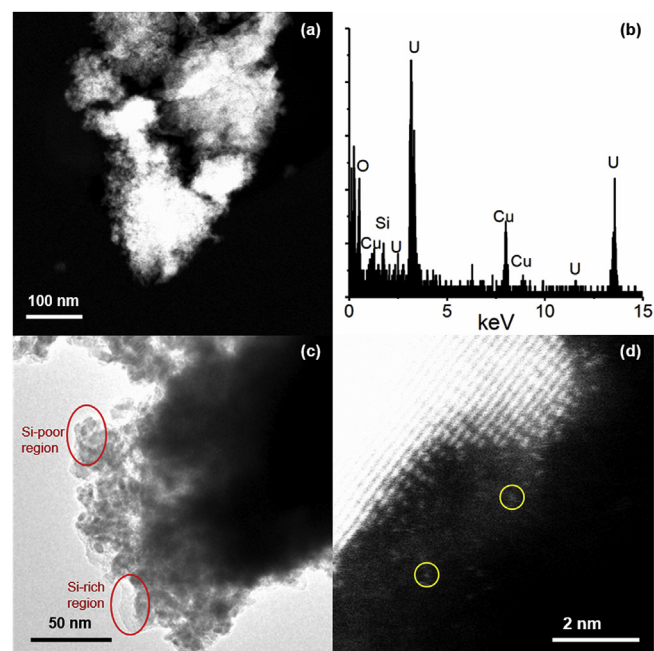


Fig. 6. Brightfield and HAADF STEM images from silicate reacted U corrosion product Experiment 1 (8.6 mM Si, 0.9 mM U) after 8 weeks. (a) High z-contrast HAADF STEM image of a particle with accompanying EDX spectrum (b) showing particle contains U and Si. (c) Standard TEM image showing variation in Si coating thickness. (d) HAADF image showing UO_2 particles (bright white) coated with a silica shell (grey) and U atoms within the silica shell (white, circled).

in the UO_2 particles is migrating into the silica coating. Indeed, it was possible to record the movement of U atoms in the silica coating (see SI video). This atomic level video contains U atoms moving under the electron beam, including atoms becoming attached and detached at the UO_2 -silica interface. This shows the UO_2 particles are undergoing a reaction with the silica coating and some U atoms are being incorporated into this non-crystalline coating. Although there were many examples of U atoms in the silica coating seen in these samples, the relative amounts of U in the silica coating compared to the UO_2 particles was very low.

Supplementary video related to this article can be found at <https://doi.org/10.1016/j.jnucmat.2019.151751>.

U L_3 edge XANES again confirmed that the majority of U was in the +4 oxidation state (Fig. S1) in all systems, and that sample oxidation had not occurred. The oxidation state of the silicate reacted U corrosion product (Experiment 1) was further probed using U M_4 edge HR-XANES, which has high sensitivity for detecting U(IV), (V) and (VI) mixed oxide states [37–39]. The HR-XANES showed that the U oxidation state is similar to that of the UO_2 standard (U(IV)), with a slight shoulder to the main peak in the spectrum at higher energy which may be due to some oxidised U present in a slightly oxidised UO_{2+x} species (Fig. S6).

EXAFS analysis and fitting for all the silicate reacted U corrosion product experiments (Fig. 1, Fig. S7 and data fits in Table 2) at both 1 and 20 weeks aging showed that the U was predominantly in a UO_2 environment with all the EXAFS spectra fit to the same UO_2 structure as the original U corrosion product sample. EXAFS from all experimental conditions were fit using 8 O backscatterers at $2.36 \pm 0.01 \text{ \AA}$, 12 U backscatterers at $3.88 \pm 0.01 \text{ \AA}$ and 24 O backscatterers at $4.46 \pm 0.02 \text{ \AA}$. Fitting parameters, including the amplitude reduction factor and energy correction, are shown in Table 2 and are within error across all systems. Additional multiple scatters (U-O-O and U-O-U pathways) were also included in the fitting and full details of these can be seen in Table S1. From the EXAFS fits it is clear that there is no detectable systematic change in the coordination of U in these systems in the presence or absence of silicate, despite the differences in particle sizes and colloidal behaviour. Overall, the fits show that the bulk U coordination environment is in agreement with U being in crystalline, nanoparticulate UO_2 in the starting material, silicate free control and silicate reacted experiments.

3.3. Silicate stabilisation of colloidal UO_2 corrosion product

Despite the apparent necessity of silicate in solution for the disaggregation of U particulates, as evidenced by 1.5–220 nm particles forming in Experiments 1–3 and not Experiment 4, there was no clear trend between the silicate concentration, or Si:U ratio, and the amount U present in the 1.5–220 nm size fraction. This suggests that even lower concentrations of silicate, not explored in this study (<1.6 mM) may also stabilise U(IV) colloids. TEM imaging (Fig. 6) shows a coating of silica on the silicate reacted U corrosion product particle surface and EXAFS shows no alteration of the UO_2 particle structure, suggesting that the silicate reaction is limited to the particle surface. As silicate is not intrinsic to the structure of the particles in this study, colloidal stability for these species appears less dependent on the silicate concentration than in previously investigated intrinsic U(IV)-silicates [13,20]. This has implications for colloidal stability of U(IV) phases in natural systems where concentrations of silicate vary from $10^{-5} - 1.6 \times 10^{-3} \text{ M}$ in groundwaters and $3 \times 10^{-5} - 1.3 \times 10^{-3} \text{ M}$ in surface waters [24]. This study shows that even the lowest investigated silicate concentrations can lead to UO_2 nanoparticle disaggregation, so it is possible that silicate stabilisation of colloidal UO_2 could occur in natural systems with moderate silicate concentrations.

The presence of 1.5–220 nm U particulates in the silicate containing systems is attributed to disaggregation of large (>220 nm), non-colloidal aggregates. Settling experiments verified that these 1.5–220 nm particulates were stable colloids, as their concentration did not decrease with increasing settling time. While the presence of silicate and the formation of a silica coating on the particles led to some disaggregation and formation of colloidal, <220 nm sized particles, the absence of U particles in the 1.5–12 nm size fraction indicates this colloid still consists of moderately aggregated particles. The source of this disaggregation and subsequent colloidal stability is the increased hydrophilicity of the particle surface. As observed for intrinsic An(IV)-silicate colloids [13,20,40], silicate present at the particle surface can increase colloidal stability by providing more favourable surface-solution interactions [41–46]. TEM showed this silica is present on the particle surface and therefore has a strong influence on surface composition, charge and colloid stability. Given these results, it is reasonable to assume that silicate was responsible for previously observed colloidal $\text{UO}_{2.08}$ which was formed from the corrosion of metallic U spent nuclear fuel under silicate rich groundwater conditions [3]. The observations from this previous study, including SAED suggested that the UO_2 particles observed are likely similar to the silicate coated U colloids in the current work. The use of high-resolution TEM and ultrafiltration has been applied in the current work to clearly identify a silica coating to the particles.

Silicate coated particles similar to those formed in this study may also be present in legacy spent nuclear fuel storage facilities. Previous investigations have found discrete black particles, characterised as UO_2 , associated with silicate in a Magnox storage pond [5]. Given the similar formation process (corrosion of metallic U at alkaline pH) these UO_2 particles likely share many characteristics with those identified in this study. It is therefore possible that these particles may be colloidal and significant transport vectors of radioactivity in effluent treatment systems at nuclear sites.

3.4. UO_2 corrosion product-silicate interactions and implications for long term fate of U(IV)

U L_3 edge and M_4 edge XAS, and XRD all suggest U in both the initial U corrosion product and the subsequent reactions with silicate, is dominated by U(IV). U M_4 edge HERFD XANES indicates U may be slightly oxidised, with a sample from silicate reacted U corrosion product (Experiment 1) being slightly altered, relative to the UO_2 standard (Fig. S6).

Despite a small amount (~0.1 ppm) of silicate present in the initial U corrosion product, the structure of this U corrosion product was still found to be UO_2 . While ultrafiltration showed association of silicate with U corrosion product particles after 1 week of reaction in Experiments 1–3, and changes in the particle size distribution, there was no change in the overall U coordination according to EXAFS fitting. This was consistent throughout the experiments in both the silicate-free and silicate containing solutions. STEM imaging supported this conclusion and showed that the Si was present as a poorly ordered, heterogeneous coating on the U corrosion product particle surface. As discussed in section 3.3., this silica coating explains how the particles are stabilised as colloids, despite relatively low ratios of Si:U in the particles, as it is highly enriched on the particle surface. There was no evidence for the presence of Si within the crystalline UO_2 regions of the U corrosion product particles, or for alteration of the bulk particle structure, showing that silicate can stabilise UO_2 particles as colloids without altering the bulk structural form of the U. While this has been observed previously for Ca-carbonates and Fe-oxyhydroxides [21,22], it has not been identified for UO_2 particles. These findings suggest that bulk analysis of the solid may not be a good representation of the

particle surface and thus the colloidal behaviour. As it is the surface that interacts with the surrounding environment, the aggregation behaviour and transport properties of the U-containing particles may be significantly different from those predicted by the bulk structure.

Atomic resolution HAADF-STEM shows evidence of U atoms in the silica coating after 8 weeks. Although the amount of U in this shell is low relative to the amount in the crystalline UO_2 particles, and therefore not detected using EXAFS, it is an interesting observation which suggests that the UO_2 surface is undergoing alteration in the presence of silica. This is significant to both the long term stabilisation of UO_2 colloids in silicate rich environments, and also the formation of alteration phases on UO_2 . If the surface alteration of UO_2 continues over longer timescales, the surface structure of these particles may become more U(IV)-silicate like. These observations are in agreement with previous work which showed coffinite-like U(IV)-silicates formed on the surface of UO_2 pellets which were exposed to silicate containing solutions [25]. The coffinite-like particles were only observed after prolonged reaction at high temperature (180 °C); however Fig. 6 suggests that isolated U atoms in an amorphous silica particle coating are the precursors to formation of U(IV)-silicates. Furthermore, the presence of UO_2 particles coated by a U(IV)-containing silica shell has similarities to the proposed core-shell structure of U(IV)-silicate colloidal particles [13]. The bulk structure of the particles formed in the current study is very different to intrinsic U(IV)-silicates, with UO_2 dominating the structure of the U corrosion product particles even when aged for 20 weeks in silicate solutions. Additionally, the formation process of the U(IV)-silicate matrix is different between these two systems, with the present study showing a reaction at the UO_2/SiO_2 interface between existing U(IV) particles and surface coatings of silica, and previous work on intrinsic U(IV)-silicates involving the reaction of dissolved U(IV) and silicate. However, over longer timescales than those explored in this study it is possible that a U(IV)-silicate structure may become increasingly prevalent. Importantly, intrinsic U(IV)-silicate particles form stable colloids [13,20], particularly under high silicate concentrations, meaning U(IV)-containing particles will remain colloidal even if their structure changes. Overall, we present clear evidence for a different formation route for U(IV)-colloids to the previously investigated intrinsic U(IV)-silicate colloids which were formed from a solution phase U(IV)-carbonate system [13,20]. This pathway represents an environmentally relevant scenario in geodisposal and spent nuclear fuel storage facilities where nano- UO_2 and silica are expected to be present.

While coffinite is abundant in the Earth's crust, its formation is poorly understood. Potential pathways to coffinite formation have been discussed and investigated previously [26–30], including oxidation/reduction processes. Natural coffinite is thought to form at temperatures between 80 and 130 °C, however most laboratory based syntheses have been carried out at higher temperatures [29] and often result in mixed UO_2 , USiO_4 and SiO_2 products. Recent studies have suggested U(IV)-silicate solution complexes and nanoparticles may play a key role in the formation of coffinite, but their role has not been comprehensively defined [13,29]. Recent investigations into the stability of uranothorites ($\text{Th}_{1-x}\text{U}_x\text{SiO}_4$) solid solutions has shown that, while U rich uranothorites (and coffinite) are unstable with respect to their binary oxides, short range ordering and favourable enthalpies can stabilise solid solutions with $x \approx 0.5$ [47]. This could also apply to U(IV) in silicates observed in the present study and previous work [13] where U(IV) is present in poorly ordered, silicate forms which may have exothermic enthalpies driving their formation and stability. This study, showing alteration of UO_2 at the UO_2 -silica interface, and subsequent migration of U(IV) into the silica coating at room

temperature, potentially provides a different pathway for the formation of U(IV)-silicates like coffinite. Further investigation of this process is required to fully understand the role of these reactions in environmental formation of U(IV)-silicates.

4. Conclusions

In summary, the product of anaerobic U metal corrosion at pH 11 was found to be UO_2 by EXAFS and XRD, consisting of crystalline nanoparticles 5–10 nm in size which formed aggregates. When reacted with silicate solutions, a fraction of the U corrosion product became colloidal and persisted for 30 weeks. The particle size and amount of colloidal U did not appear to be dependent on the silicate concentration in solution. No colloidal U was found in the silicate free experiment, suggesting silicate is essential for formation of UO_2 -based colloids. XAS and STEM showed that reactions with silicate resulted in the formation of a silica coating, with little change in the bulk UO_2 structure. Atomic resolution STEM showed evidence of surface alteration of the U-containing particles with migration of U atoms into the amorphous silica-like coating as non-crystalline U(IV). These results demonstrate that silicate can stabilise UO_2 as a colloid under environmentally relevant concentrations at a pH representative of both spent nuclear fuel storage and geodisposal scenarios. While the bulk structure shows little change over 30 weeks, evidence of UO_2 alteration at the UO_2 -silica interface suggests that these conditions could lead to eventual U(IV)-silicate formation.

Data availability

The raw/processed data required to reproduce these findings cannot be shared at this time due to technical or time limitations.

Acknowledgements

The University of Manchester, Sellafield Ltd., and the National Nuclear Laboratory co-funded this work via the Effluents and Decontamination Centre of Expertise. The research was also supported through an EPSRC impact acceleration project (EP/R511626/1). The National Nuclear Laboratory provided additional funding via the Environmental Radiochemistry Core Science theme. A part of this work was performed at the William R. Wiley Environmental Molecular Science Laboratory (EMSL) sponsored by the US Department of Energy, Office of Biological and Environmental Research located at Pacific Northwest National Laboratory (PNNL) under science theme proposal 49774. We thank EMSL staff for their assistance. Diamond Light Source provided beamtime access via awards (SP17243), and we thank Steven Parry and Giannantonio Cibin for beamline assistance. We also thank Paul Lythgoe, and Heath Bagshaw for data acquisition. We acknowledge beamtime access for m-edge spectroscopy at the KIT synchrotron radiation source, CATACT and thank Jurij Galanzew and Joerg Rothe for beamtime assistance.

Appendix A. Supplementary data

Supplementary data to this article can be found online at <https://doi.org/10.1016/j.jnucmat.2019.151751>.

References

- [1] J. Bruno, R.C. Ewing, Spent nuclear fuel, *Elements* 2 (6) (2006) 343–349, <https://doi.org/10.2113/gselements.2.6.343>.
- [2] E.L. Fuller, et al., Uranium Oxidation: Characterization of Oxides Formed by Reaction with Water by Infrared and Sorption Analyses, vol 120, 1984, pp. 174–194, [https://doi.org/10.1016/0022-3115\(84\)90056-4](https://doi.org/10.1016/0022-3115(84)90056-4).

- [3] M.D. Kaminski, et al., Colloids from the aqueous corrosion of uranium nuclear fuel, *J. Nucl. Mater.* 347 (1–2) (2005) 77–87, <https://doi.org/10.1016/j.jnucmat.2005.07.009>.
- [4] S.I. Sinkov, C.H. Delegard, A.J. Schmidt, Preparation and Characterization of Uranium Oxides in Support of the K Basin Sludge Treatment Project, PNNL17678. Richland, WA, 2008, <https://doi.org/10.2172/940228>.
- [5] C.R. Gregson, et al., Combined electron microscopy and vibrational spectroscopy study of corroded Magnox sludge from a legacy spent nuclear fuel storage pond, *J. Nucl. Mater.* 412 (1) (2011) 145–156, <https://doi.org/10.1016/j.jnucmat.2011.02.046>. Elsevier B.V.
- [6] R.L. Segall, R.S.C. Smart, P.S. Turner, Oxide surfaces in solution, in: J. Nowotny, L.C. Dufour (Eds.), *Surface and Near-Surface Chemistry of Oxide Materials*, Elsevier, Amsterdam, 1988, p. 527, <https://doi.org/10.1177/1087057105284339>.
- [7] D.R. Lovley, et al., Microbial reduction of uranium, *Nature* 350 (6317) (1991) 413–416, <https://doi.org/10.1038/350413a0>.
- [8] L. Newsome, K. Morris, J.R. Lloyd, The biogeochemistry and bioremediation of uranium and other priority radionuclides, *Chem. Geol.* 363 (2014) 164–184, <https://doi.org/10.1016/j.chemgeo.2013.10.034>.
- [9] D. Langmuir, *Aqueous Environmental Geochemistry*, Prentice Hall, New Jersey, 1997.
- [10] H. Zänker, C. Hennig, Colloid-borne forms of tetravalent actinides: a brief review, *J. Contam. Hydrol.* 157 (2014) 87–105, <https://doi.org/10.1016/j.jconhyd.2013.11.004>. Elsevier B.V.
- [11] Y. Wang, et al., Mobile uranium(IV)-bearing colloids in a mining-impacted wetland, *Nat. Commun.* 4 (May) (2013) 1–9, <https://doi.org/10.1038/ncomms3942>. Nature Publishing Group.
- [12] A.B. Kersting, et al., Migration of plutonium in ground water at the Nevada Test Site, *Nature* 397 (6714) (1999) 56–59, <https://doi.org/10.1038/16231>.
- [13] T.S. Neill, et al., Stability, composition, and core-shell particle structure of uranium(IV)-Silicate colloids, *Environ. Sci. Technol.* 52 (16) (2018) 9118–9127, <https://doi.org/10.1021/acs.est.8b01756>.
- [14] Z. Maher, et al., Americium and plutonium association with magnesium hydroxide colloids in alkaline nuclear industry process environments, *J. Nucl. Mater.* 468 (2016) 84–96, <https://doi.org/10.1016/j.jnucmat.2015.11.010>. Elsevier B.V.
- [15] A. van Veen, et al., Uranium uptake onto Magnox sludge minerals studied using EXAFS, *Mineral. Mag.* 76 (8) (2012) 3095–3104, <https://doi.org/10.1180/minmag.2012.076.8.24>.
- [16] A.J. Popel, et al., Surface alteration evidence for a mechanism of anoxic dissolution of UO₂, *Appl. Surf. Sci.* 464 (2019) 376–379, <https://doi.org/10.1016/j.apsusc.2018.09.094>. Elsevier, (June 2018).
- [17] V. Neck, J.I. Kim, Solubility and hydrolysis of tetravalent actinides, *Radiochim. Acta* 89 (1) (2001) 1–16, <https://doi.org/10.1524/ract.2001.89.1.001>.
- [18] K. Opel, et al., Study of the solubility of amorphous and crystalline uranium dioxide by combined spectroscopic methods, *Radiochim. Acta* 95 (3) (2007) 143–149, <https://doi.org/10.1524/ract.2007.95.3.143>.
- [19] A. Husain, Charge development at the uranium oxide-solution interface, *J. Colloid Interface Sci.* 102 (2) (1984) 389–399, [https://doi.org/10.1016/0021-9797\(84\)90241-8](https://doi.org/10.1016/0021-9797(84)90241-8).
- [20] I. Dreissig, et al., Formation of uranium(IV)-silica colloids at near-neutral pH, *Geochim. Cosmochim. Acta* 75 (2) (2011) 352–367, <https://doi.org/10.1016/j.gca.2010.10.011>.
- [21] E. Doelsch, et al., Chemistry and structure of colloids obtained by hydrolysis of Fe(III) in the presence of SiO₄ ligands, *Colloid. Surf. Physicochem. Eng. Asp.* 217 (1–3) (2003) 121–128, [https://doi.org/10.1016/S0927-7757\(02\)00566-6](https://doi.org/10.1016/S0927-7757(02)00566-6).
- [22] M. Kellermeier, et al., Colloidal stabilization of calcium carbonate pre-nucleation clusters with silica, *Adv. Funct. Mater.* 22 (20) (2012) 4301–4311, <https://doi.org/10.1002/adfm.201200953>.
- [23] J. Janeczek, R.C. Ewing, Dissolution and alteration of uraninite under reducing conditions, *J. Nucl. Mater.* 190 (C) (1992) 157–173, [https://doi.org/10.1016/0022-3115\(92\)90084-X](https://doi.org/10.1016/0022-3115(92)90084-X).
- [24] R. Siever, Silicon abundance in natural waters, in: K.H. Wedepohl (Ed.), *Handbook of Geochemistry*, vol. 2, 1972.
- [25] M. Amme, et al., Uranium secondary phase formation during anoxic hydrothermal leaching processes of UO₂ nuclear fuel, *J. Nucl. Mater.* 341 (2–3) (2005) 209–223, <https://doi.org/10.1016/j.jnucmat.2005.02.004>.
- [26] S. Szenknect, et al., From uranothorites to coffinite: a solid solution route to the thermodynamic properties of USiO₄, *Inorg. Chem.* 52 (12) (2013) 6957–6968, <https://doi.org/10.1021/ic400272s>.
- [27] S. Labs, et al., Synthesis of coffinite, USiO₄, and structural investigations of UxTh(1–x)SiO₄ solid solutions, *Environ. Sci. Technol.* 48 (1) (2014) 854–860, <https://doi.org/10.1021/es403995b>.
- [28] X. Guo, et al., Thermodynamics of formation of coffinite, USiO₄, *Proc. Natl. Acad. Sci.* 112 (21) (2015) 6551–6555, <https://doi.org/10.1073/pnas.1507441112>.
- [29] A. Mesbah, et al., Coffinite, USiO₄, is abundant in nature: so why is it so difficult to synthesize? *Inorg. Chem.* 54 (14) (2015) 6687–6696, <https://doi.org/10.1021/jc502808n>.
- [30] S. Szenknect, et al., First experimental determination of the solubility constant of coffinite, *Geochim. Cosmochim. Acta* 181 (2016) 36–53, <https://doi.org/10.1016/j.gca.2016.02.010>.
- [31] K.A. Granath, Solution properties of branched dextrans, *J. Colloid Sci.* 13 (4) (1958) 308–328, [https://doi.org/10.1016/0095-8522\(58\)90041-2](https://doi.org/10.1016/0095-8522(58)90041-2).
- [32] T.C. Laurent, K. a Granath, Fractionation of dextran and ficoll by chromatography on sephadex G-200, *Biochim. Biophys. Acta Gen. Subj.* 136 (2) (1967) 191–198, [https://doi.org/10.1016/0304-4165\(67\)90063-3](https://doi.org/10.1016/0304-4165(67)90063-3).
- [33] B. Ravel, M. Newville, 'ATHENA', 'ARTEMIS', 'HEPHAESTUS': data analysis for X-ray absorption spectroscopy using IFEFFIT, *J. Synchrotron Radiat. Int. Union Crystallogr.* 12 (4) (2005) 537–541, <https://doi.org/10.1107/S0909049505012719>.
- [34] A. Zimina, et al., CAT-ACT—a new highly versatile x-ray spectroscopy beamline for catalysis and radionuclide science at the KIT synchrotron light facility ANKA, *Rev. Sci. Instrum.* 88 (11) (2017) 113113, <https://doi.org/10.1063/1.4999928>.
- [35] J. Janeczek, R.C. Ewing, X-ray powder diffraction study of annealed uraninite, *J. Nucl. Mater.* 185 (1) (1991) 66–77, [https://doi.org/10.1016/0022-3115\(91\)90366-F](https://doi.org/10.1016/0022-3115(91)90366-F).
- [36] R. Guillaumont, et al., Update on the chemical thermodynamics of uranium, neptunium, plutonium, americium and technetium, *Chem. Thermodyn.* 5 (2003) 919.
- [37] G. Leinders, et al., Evolution of the uranium chemical state in mixed-valence oxides, *Inorg. Chem.* 56 (12) (2017) 6784–6787, <https://doi.org/10.1021/acs.inorgchem.7b01001>.
- [38] I. Pidchenko, et al., Uranium redox transformations after U(VI) coprecipitation with magnetite nanoparticles, *Environ. Sci. Technol.* 51 (4) (2017) 2217–2225, <https://doi.org/10.1021/acs.est.6b04035>.
- [39] H.E. Roberts, et al., Uranium(V) incorporation mechanisms and stability in Fe(II)/Fe(III) (oxyhydr)Oxides, *Environ. Sci. Technol. Lett.* 4 (10) (2017) 421–426, <https://doi.org/10.1021/acs.estlett.7b00348>.
- [40] H. Zänker, et al., Oxyhydroxy silicate colloids: a new type of waterborne actinide(IV) colloids, *ChemistryOpen* 5 (3) (2016) 174–182, <https://doi.org/10.1002/open.201500207>.
- [41] H. Yotsumoto, R.-H. Yoon, Application of extended DLVO theory: II. Stability of silica suspensions, *J. Colloid Interface Sci.* (1993) 434–441, <https://doi.org/10.1006/jcis.1993.1206>.
- [42] J.-P. Chapel, Electrolyte species dependent hydration forces between silica surfaces, *Langmuir* 10 (11) (1994) 4237–4243, <https://doi.org/10.1021/la00023a053>.
- [43] L.K. Koopal, Mineral hydroxides: from homogeneous to heterogeneous modelling, *Electrochim. Acta* 41 (1996) 2293–2306, [https://doi.org/10.1016/0013-4686\(96\)00059-X](https://doi.org/10.1016/0013-4686(96)00059-X) (14 SPEC. ISS.).
- [44] D. Grasso, et al., A review of non-DLVO interactions in environmental colloidal systems, *Rev. Environ. Sci. Biotechnol.* 1 (1) (2002) 17–38, <https://doi.org/10.1023/A:1015146710500>.
- [45] J.J. Valle-Delgado, et al., Hydration forces between silica surfaces: experimental data and predictions from different theories, *J. Chem. Phys.* 123 (3) (2005) 034708, <https://doi.org/10.1063/1.1954747>.
- [46] A.-C.J.H. Johnson, et al., Aggregation of nanosized colloidal silica in the presence of various alkali cations investigated by the electrospray technique, *Langmuir* 24 (22) (2008) 12798–12806, <https://doi.org/10.1021/la8026122>.
- [47] X. Guo, et al., Energetics of a uranothorite (Th_{1-x}U_xSiO₄) solid solution, *Chem. Mater.* 28 (19) (2016) 7117–7124, <https://doi.org/10.1021/acs.chemmater.6b03346>.